J Solid State Electrochem (2012) 16:3115–3122
DOI 10.1007/s10008-012-1753-0

ORIGINAL PAPER

Preparation, characterization, and electrochemical studies of sulfur-bearing nickel in an ammoniacal electrolyte: the influence of thiourea

Huazhen Cao · Di Yang · Shili Zhu · Li Dong · Guoqu Zheng

Received: 23 November 2011 / Revised: 12 April 2012 / Accepted: 15 April 2012 / Published online: 3 May 2012
© Springer-Verlag 2012

Abstract Sulfur-bearing nickel was prepared by a direct electrodeposition in an ammoniacal Ni(II) electrolyte containing thiourea. This sulfur-bearing nickel showed an excellent dissolving activity when used as anodic materials in the traditional Watt bath. The influence of thiourea on the surface microstructure, crystallization texture, and electrocrystallization process of sulfur-bearing nickel were investigated by scanning electron microscopy, X-ray diffraction, and electrochemical techniques. The results show that the S element is uniformly distributed in the electrodeposited nickel. The prepared nickel samples present a blade shape microstructure, and the blade size decreases by the addition of thiourea. Sulfur-bearing nickel exhibits face-centered cubic structure and (111) preferred orientation, and the orientation distribution is strengthened with increased thiourea concentration. The nucleation parameters, such as N_0, A, and J_0, are obtained from the initial parts of the transients making use of Sharifker–Mostany theoretical model. Both the nucleation rate and the vertical growth rate are increased by the addition of thiourea, leading to finer grains and better dissolving activity.

Keywords Thiourea · Sulfur-bearing nickel · Crystal structure · Electrocrystallization

Introduction

Dissolving performance of an anodic material is one of the most important factors which influence the quality of coating. The active nickel containing sulfur has received extensive attention in nickel electroplating industry due to the low dissolution potential and no passivation on the surface. For the fabrication of sulfur-bearing nickel, a liquid phase sintering process has been developed 20 years ago, using high purity nickel powder as material [1]. These anodes led to good electroplate and very little residue. Electrodeposition, as a simple method, was also introduced in the preparation of sulfur-bearing nickel [2–5]. In this method, additives such as thiourea and saccharin are commonly added to the nickel electrolytes, which are easy to be incorporated in nickel deposits owing to its strong adsorbability and its consequent influence on the interfacial characteristics.

Up to now, in the studies on the electrodeposition of sulfur-bearing Ni concentrated on acidic medium [6, 7], no corresponding research in ammoniacal medium has been reported. As well-known, ammoniacal leaching solution has been widely used in hydrometallurgical processes due to its inherent advantages [8–10]. For example, the components like iron, calcium, aluminum, silicon, etc. can be removed during the leaching step as insoluble oxy/hydroxyl compounds. This allows selective extraction of the valuable metals as soluble ammonia complexes, so the product has a high purity. In this work, we combined thiourea with ammoniacal Ni(II) electrolyte to prepare the sulfur-bearing nickel with high activity by direct electrodeposition.

Electrodeposition process is normally associated with nucleation and crystal growth. The higher the nucleation rate, the finer the crystal grains grow. The mechanism of nucleation and growth determines the surface morphology and microstructure of the deposits as well as its properties. Chronoamperometric transient is a powerful electrochemical method to study the heterogeneous nucleation [11–15], in which the driving force for nucleation can be varied simply by turning the applied potential. A number of theoretical

H. Cao · D. Yang · S. Zhu · L. Dong · G. Zheng (✉)
College of Chemical Engineering and Materials Science,
Zhejiang University of Technology,
Chaowang Road, 18,
Hangzhou 310014, People's Republic of China
e-mail: zhenggq@zjut.edu.cn

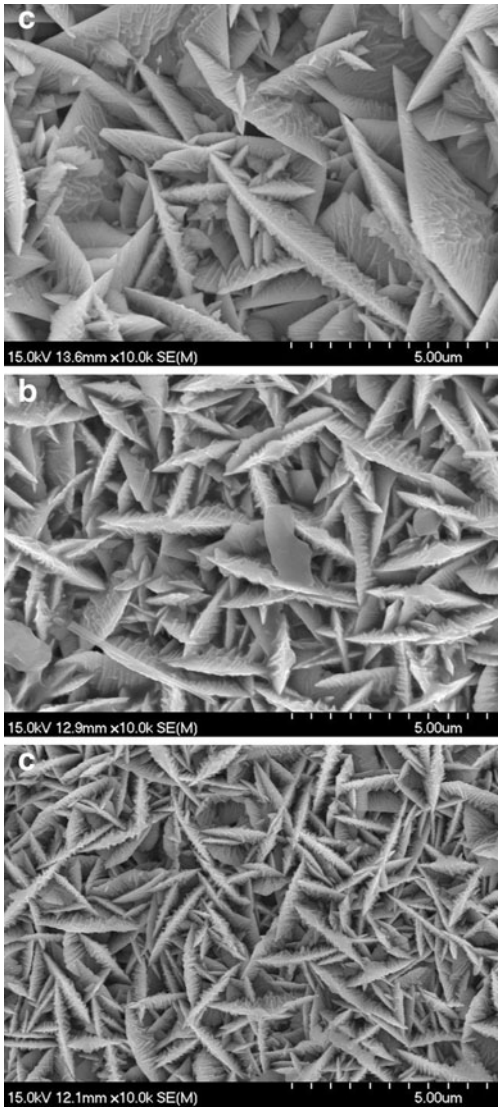

Fig. 1 Surface morphology of nickel samples electrodeposited from the solutions containing 1 mol L^{-1} $NiCl_2$, 4 mol L^{-1} NH_4Cl, 4 mol L^{-1} NH_3 (aq), and **a** 0 g L^{-1} thiourea, **b** 0.02 g L^{-1} thiourea, and **c** 0.04 g L^{-1} thiourea. Electrodeposition time 2 h, temperature 60 °C, current density 40 mA cm^{-2}

studies on nucleation kinetics were conducted based on this method [16–19]. In this paper, the fundamental of how thiourea influences the metallic electrocrystallization was discussed by chronoamperometry method. The information regarding the effect of thiourea on the properties and structure

Table 1 Contents of S in nickel deposits

Thiourea concentration in electrolyte (g L^{-1})	Sulfur content in nickel deposits (%)
0	0
0.02	0.14
0.04	0.20

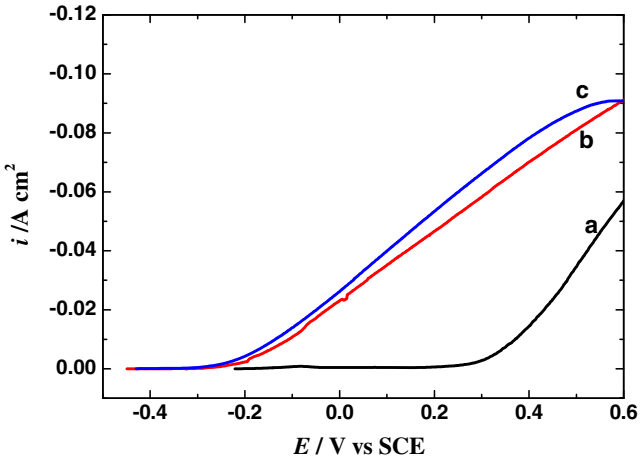

Fig. 2 Anodic polarization curves of nickel samples electrodeposited from the solutions containing 1 mol L^{-1} $NiCl_2$, 4 mol L^{-1} NH_4Cl, 4 mol L^{-1} NH_3 (aq), and *a* 0 g L^{-1} thiourea, *b* 0.02 g L^{-1} thiourea, and *c* 0.04 g L^{-1} thiourea

of as-deposited sulfur-bearing Ni was also achieved by the characterization based on X-ray diffraction (XRD) and scanning electron microscopy (SEM) measurement.

Experimental

Samples, preparation, and characterization

Sulfur-bearing nickel samples were prepared by direct electrodeposition on stainless steel substrate in the galvanostatic regime. The electrolytes were prepared by adding thiourea to a solution with 1 mol L^{-1} $NiCl_2$, 4 mol L^{-1} NH_4Cl, and 4 mol L^{-1} NH_3 (aq), in which the dominant nickel specie is $Ni(NH_3)_4^{2+}$ according to the thermodynamic analysis [20].

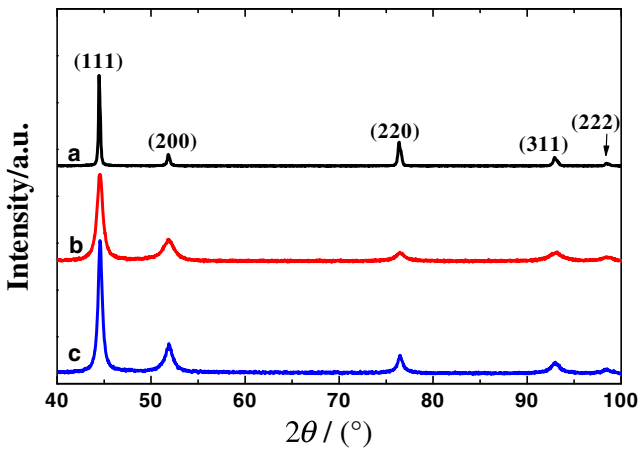

Fig. 3 XRD patterns of nickel samples electrodeposited from the solutions containing 1 mol L^{-1} $NiCl_2$, 4 mol L^{-1} NH_4Cl, 4 mol L^{-1} NH_3 (aq), and *a* 0 g L^{-1} thiourea, *b* 0.02 g L^{-1} thiourea, and *c* 0.04 g L^{-1} thiourea

All solutions were freshly prepared just before the beginning of each series of experiments. Electrodeposition was performed at 60 °C for 2 h with a current density of 40 mA cm^{-2}.

XRD patterns were recorded by an X/Pert PRO X-ray diffractometer using Cu-Kα radiation. The surface morphology of nickel sample was observed by Hitachi S-4700 field emission scanning electron microscopy at accelerating voltage of 200 kV. Sulfur distribution in nickel sample was investigated by Noran energy dispersive X-ray spectroscopy (EDS). The content of sulfur in nickel sample was measured with an X-ray fluorescence spectrometry.

Electrochemical measurements

A three-electrode glass cell, consisting of a working electrode, a reference electrode (saturated calomel electrode), and a counter electrode (platinum wire), was used for electrochemical measurements. Anodic polarization curves for nickel samples in the traditional Watt bath were recorded to determine the anodic dissolving performance. The potential was shifted from open potential to 600 mV (vs SCE) with a scan rate of 1 mV s^{-1}.

Cyclic voltammetric and chronoamperometric measurements were performed in the ammoniacal Ni(II) electrolyte with different contents of thiourea, in order to study the electrocrystallization process. A glassy carbon electrode (exposure area 0.1256 cm^2) was used as working electrode in this measurement. All electrochemical tests were carried out on an EG&G 273 Potentiostat/Galvanostat.

Results and discussion

Surface morphology and composition of nickel samples

Figure 1 shows the surface morphology of nickel samples obtained by electrodeposition in the ammoniacal Ni(II) electrolyte with different content of thiourea. It is observed that all samples exhibit a blade shape microstructure. The blade size of nickel sample obtained in the absence of thiourea is around 5 μm in length, while it dramatically decreased to less than 3.5 μm when 0.02 g L^{-1} thiourea was added. Also with the increase of thiourea concentration, the blade size tends to further reduce. It is clear that the addition of thiourea affects the electrodeposition of nickel, leading to the finer grain. EDS analysis proves that the sulfur distribution is uniform. The contents of sulfur in different samples are listed in Table 1. With the increased thiourea concentration, the content of sulfur in nickel deposits increases, and the mass ratio of sulfur reach 0.2 % when the concentration of thiourea in electrolyte is 0.04 g L^{-1}.

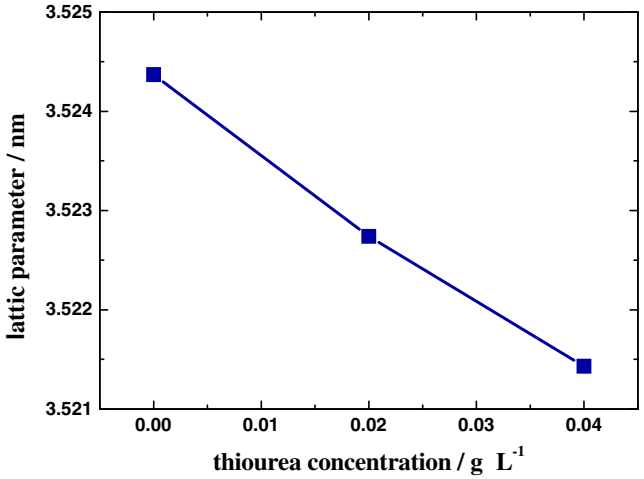

Fig. 4 Effect of thiourea concentration on the lattice parameter of electrodeposited nickel

Anodic behavior of as-prepared sulfur-bearing nickel in Watt bath

In order to determine the anodic dissolving performance of as-prepared sulfur-bearing nickel in Watt bath, anodic polarization curves were measured and shown in Fig. 2. For the

Table 2 XRD results of nickel samples prepared at various thiourea concentrations

Thiourea concentration (g L^{-1})		Face of crystal index				
		(111)	(200)	(220)	(311)	(222)
0	2θ (deg)	44.476	51.804	76.376	92.913	98.453
	I/I_0	100	11.9	27.4	10	3.3
	TC (%)	65.5	7.80	18.0	6.55	2.16
0.02	2θ (deg)	44.483	51.867	76.463	93.043	98.359
	I/I_0	100	19.2	9.3	8.5	4.9
	TC (%)	70.5	13.5	6.55	5.99	3.45
0.04	2θ (deg)	44.483	51.822	76.431	93.017	98.312
	I/I_0	100	19.4	7.4	7.9	5.0
	TC (%)	71.6	13.9	5.30	5.65	3.60

nickel prepared in solution without thiourea, the onset potential for dissolution is about 0.25 V, while it shifts to a more negative value (−0.25 V) when the sample is prepared from the electrolyte containing 0.02 g L^{-1} thiourea which can offer around 0.14 % sulfur to the sample. Anodic polarization behavior indicates that the sulfur-bearing nickel has high anodic dissolving activity in Watt bath and the activity increases with the increasing of sulfur content. The high anodic dissolving activity might be explained by the effects of heterogeneous impurity. Usually, the dissolution of a metal begins at the place where atom is irregularly arranged and then propagates along lattice boundary. The existence of heterogeneous impurity in nickel interferes with the arrangement of nickel atoms, which increases anodic dissolution. The more the amount of heterogeneous impurity sulfur, the faster the nickel is inclined to dissolve. In addition, as evidenced by Fig. 1, the nickel crystal grain decreases with the addition of thiourea, leading to more borderline, which might be another reason for the high anodic dissolving activity.

Crystal structure

The influence of thiourea on the crystal structure of electrodeposited nickel was investigated by XRD patterns, and results are presented in Fig. 3. All the XRD patterns show typical peaks corresponding to (111), (200), (220), (311), and (222) crystallographic planes of nickel, indicating that all samples have a face-centered cubic structure. For all the nickel samples, the intensity of (111) peaks is the highest, indicating the preferred orientation of (111) plane parallel to the deposits surface. Figure 4 shows the relationship between the lattice parameters of these nickel samples and thiourea concentration. With the increase of thiourea concentration, lattice parameter of electrodeposited nickel decreases. The nickel deposit includes complete lattice area and all kinds of defects. The existence of impurity, such S, leads to forming more lattice defects. The number of these defects increases with the increased thiourea concentration. So the proportion of distortion lattice near the defects area increases and the lattice parameter decreases accordingly.

Detailed analysis of XRD patterns is necessary to understand the effect of thiourea on the microstructure of electrodeposited nickels. To quantify the relative crystallographic textures associated with nickel samples

Table 3 Effect of thiourea concentration on the grain size of electrodeposited Ni

Thiourea concentration (g L^{-1})	0	0.02	0.04
Gain size (nm)	43.0	13.7	11.3

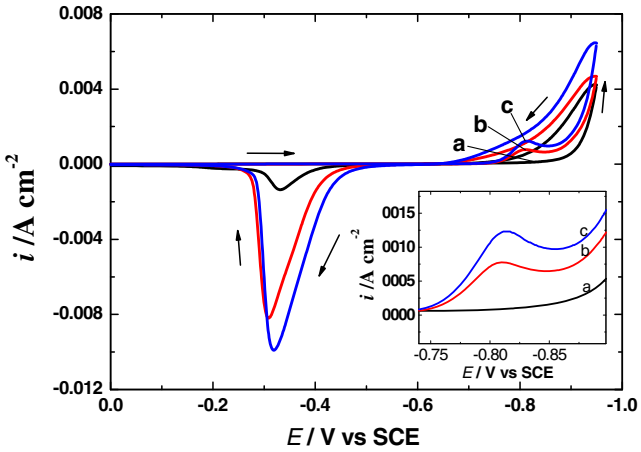

Fig. 5 Cyclic voltammetry curves obtained in the aqueous solutions containing 1 mol L^{-1} $NiCl_2$, 4 mol L^{-1} NH_4Cl, 4 mol L^{-1} NH_3 (aq), and *a* 0 g L^{-1} thiourea, *b* 0.02 g L^{-1} thiourea, and *c* 0.04 g L^{-1} thiourea at scan rate of 130 mV s^{-1}

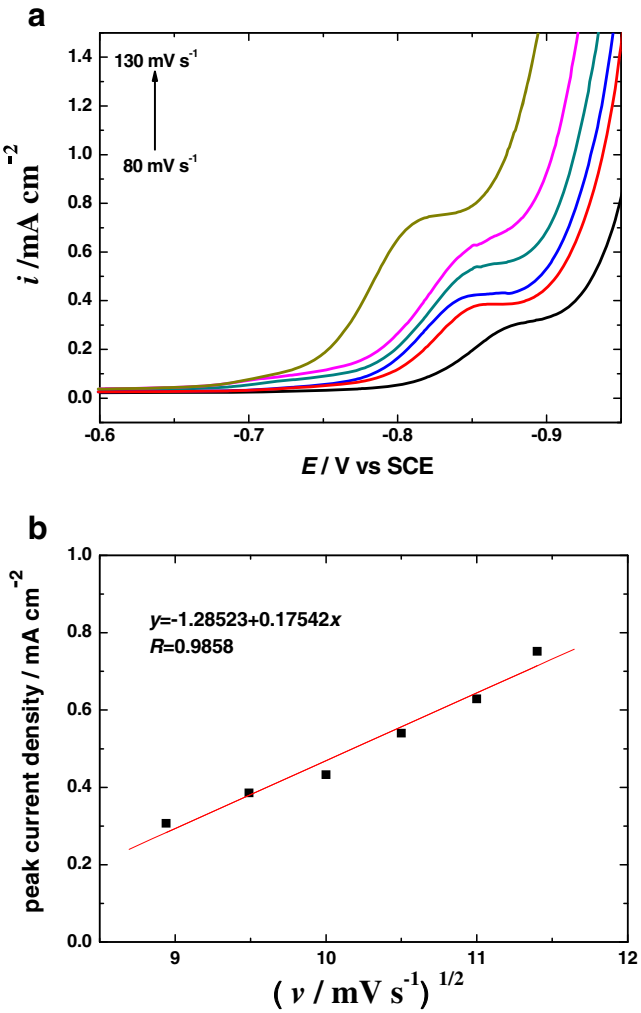

Fig. 6 **a** Linear sweep voltammetry curves obtained in the solution containing 1 mol L^{-1} $NiCl_2$, 4 mol L^{-1} NH_4Cl, 4 mol L^{-1} NH_3 (aq), and 0.02 g L^{-1} thiourea at scan rate of 80–130 mV s^{-1}. **b** Dependence of peak current density on $v^{1/2}$

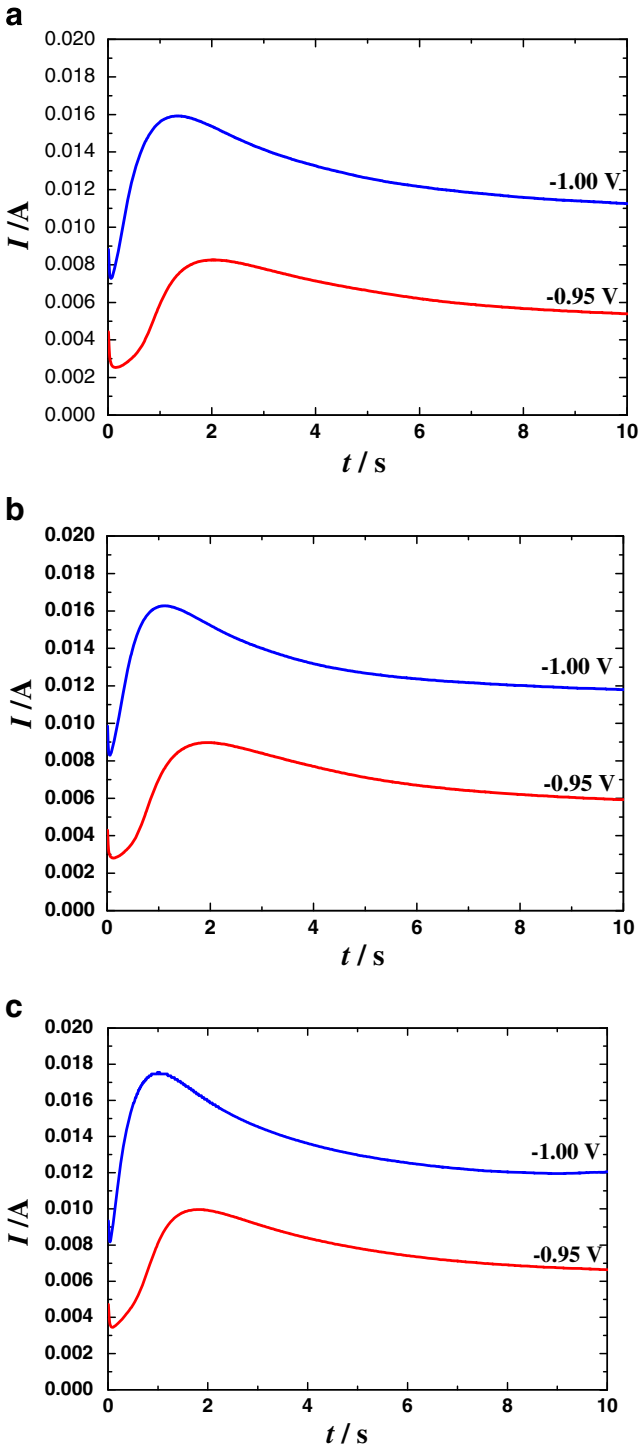

Fig. 7 Experimental current transients for nickel electrocrystallization on vitreous carbon at different applied potentials from the aqueous solutions containing 1 mol L^{-1} $NiCl_2$, 4 mol L^{-1} NH_4Cl, 4 mol L^{-1} NH_3 (aq), and **a** 0 g L^{-1} thiourea, **b** 0.02 g L^{-1} thiourea, and **c** 0.04 g L^{-1} thiourea

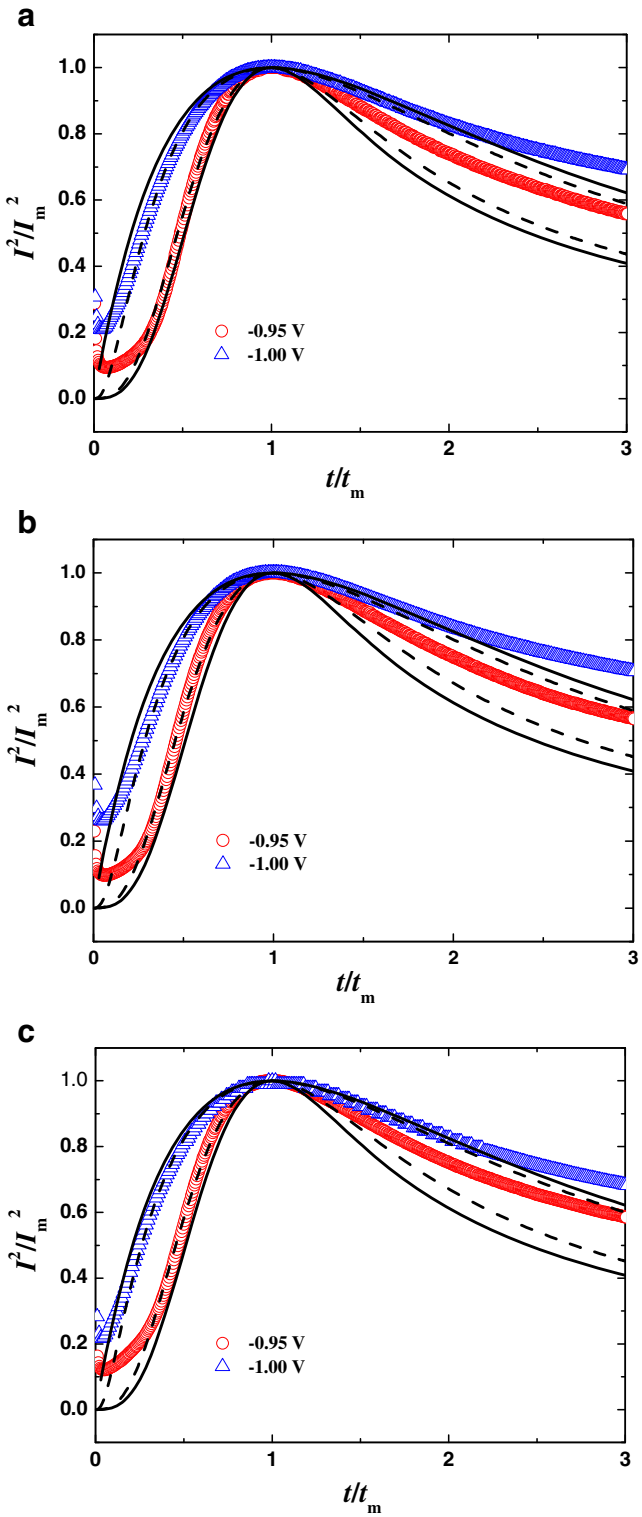

Fig. 8 Experimental (*dot*) and calculated (*dash curve*) non-dimensional plots of $I^2/I_m^2 \sim t/t_m$ together with the corresponding plots for instantaneous nucleation (*upper continuous curve*) and progressive nucleation (*lower continuous curve*). **a** 0 g L^{-1} thiourea, **b** 0.02 g L^{-1} thiourea, and **c** 0.04 g L^{-1} thiourea

and orientation of the atomic arrangement, texture coefficients (TC) for predominant (*hkl*) peaks in XRD patterns were calculated. The texture coefficient for each (*hkl*) reflection is given by $TC(hkl) = \frac{I(hkl)}{I_0(hkl)} \times \left[\sum_{i=1}^{n} \frac{I(hkl)}{I_0(hkl)}\right]^{-1}$, where $I(hkl)$ is measured intensities of (*hkl*) reflection, $I_0(hkl)$ is powder diffraction intensities of nickel, and n is the number of reflections used in the calculations. In this case, (111), (200), (220), (311), and (222) reflections were considered for texture coefficient calculation (n=5). Table 2 summarizes the results of texture coefficient calculations for the five reflections of nickel samples prepared at various thiourea concentrations. For the nickel sample containing sulfur, the (111), (200), (222) texture coefficients, especially (111) texture coefficient, are increased. While the (220), (311) texture coefficients are decreased, indicating strong (111) crystallographic texture and inhibitory action in (220).

The crystal size of the nickel sample was calculated by Scherer equation, $d = \frac{\kappa\lambda}{B\cos\theta_0}\frac{180}{\pi}$, where d is the crystallite size in nanometers, θ_0 the diffraction angle, B the full width half maxima in $2\theta_0$ degrees, κ the camera constant evaluated as 0.94, and λ the wavelength of the radiation used. The calculated results are presented in Table 3. For the sample obtained in electrolyte without thiourea, the crystallite size is about 43 nm, while it is dramatically reduced when thiourea is added. It is also observed that the crystallite size is slightly decreased with the increasing of thiourea concentration.

Electrochemical studies

Cyclic voltammograms (CV) for nickel electrodeposition on a vitreous carbon electrode at different thiourea concentrations are presented in Fig. 5. It can be found that the metallic nickel starts to deposit at a potential lower than −700 mV. In each case, the CV exhibits a nucleation loop in which more cathode current flows after the scan is reversed, very typical for nucleation and growth processes [21]. It is noted that in the electrolyte containing 0.02 g L^{-1} thiourea, a cathodic peak corresponding to the reduction of nickel appears at about −800 mV, which is not found in the electrolyte without thiourea. The cathodic peak becomes stronger when thiourea concentration is increased to 0.04 g L^{-1}, indicating an acceleration effect by thiourea in the reduction process. Some literature has reported [22] that reactive intermediate can be formed from thiourea during the deposition, which facilitates the transfer of electrons to the nickel ions and enables acceleration of the deposition at low concentration of thiourea.

Figure 6 shows a set of voltammograms obtained at different scan rates. Linear relationship is observed between peak current density and square root of scan rate with a correlation coefficient of 0.9858 in the range from 80 to 130 mV s^{-1}, which indicates that the reduction process is controlled by diffusion [23]. A family of potentiostatic current transients recorded during nickel electrodeposition from electrolytes with various thiourea concentrations are shown in Fig. 7. The shape of these transients shows a typical response of nucleation and growth process occurring under the mass transport control [24, 25]. The cathode current density abruptly increases after double layer charging at very short time. Once the current maximum was reached, a decay of the current was obtained, which approaches asymptotically the Cottrell equation.

Multiple nucleation and diffusion-controlled growth model proposed by Scharifker and Hills [24] allows classifying the nucleation and growth mechanism as instantaneous nucleation (Eq. (1)) or progressive nucleation (Eq. (2)). In the first case, the nucleation rate is very high, and in the latter case, the nucleation rate has a low value.

$$I = \frac{zFD^{1/2}C}{\pi^{1/2}t^{1/2}}[1 - \exp(-N_0\pi kDt)] \quad (1)$$

$$I = \frac{zFD^{1/2}C}{\pi^{1/2}t^{1/2}}\left[1 - \exp\left(-A\pi k'Dt^2/2\right)\right] \quad (2)$$

where zF is the molar charge transferred during electrodeposition, D the diffusion coefficient, C the bulk concentration, N_0 the number of active sites on the substrate, A the nucleation rate constant, and κ, κ' the constant decided by experiment. From the time-dependent current density expressions, one can

Table 4 Calculated values for D, N_0, A, and J_0 at various potentials and various thiourea concentrations

Thiourea concentration (g L^{-1})	E (V)	t_m (s)	I_m (A cm^{-2})	D (cm^2 s^{-1})	A (s^{-1})	N_0 (cm^{-2})	J_0 (cm^{-2} s^{-1})
0	−0.95	2.03	0.0657643	1.0×10^{-6}	0.6019	1.94×10^{6}	1.17×10^{6}
	−1.00	1.34	0.1268312	3.3×10^{-6}	13.35247	0.25×10^{6}	3.34×10^{6}
0.02	−0.95	1.95	0.0714172	1.1×10^{-6}	0.93141	1.28×10^{6}	1.19×10^{6}
	−1.00	1.12	0.1295382	2.9×10^{-6}	15.97528	0.35×10^{6}	5.59×10^{6}
0.04	−0.95	1.82	0.0792994	1.3×10^{-6}	0.99794	1.19×10^{6}	1.19×10^{6}
	−1.00	1.01	0.1398089	3.1×10^{-6}	27.08976	0.34×10^{6}	9.21×10^{6}

get the I_m at $t=t_m$ and then the dimensionless equations for two different growth mechanisms are derived:

For instantaneous nucleation growth

$$I^2/I_m^2 = \frac{1.9542}{t/t_m}\{1-\exp[-1.2564(t/t_m)]\}^2 \quad (3)$$

For progressive nucleation growth

$$I^2/I_m^2 = \frac{1.2254}{t/t_m}\left\{1-\exp\left[-2.3367(t/t_m)^2\right]\right\}^2 \quad (4)$$

Figure 8 shows the experimental plots of I^2/I_m^2 versus t/t_m with those obtained from the theoretical expression Eqs. (3) and (4). It is observed that the dimensionless curves obtained from experimental data exist between the two theoretical curves. Qualitative description of the experimental data was conducted in terms of Sharifker–Mostany theoretical model [25]

$$\ln\left(1-I_m t_m^{1/2}/a\right)+x-\alpha\left(1-e^{-x/\alpha}\right)=0 \quad (5)$$

$$\ln\left[1+2x\left(1-e^{-x/\alpha}\right)\right]-x+\alpha\left(1-e^{-x/\alpha}\right)=0 \quad (6)$$

where $a=zFD^{1/2}C/\pi^{1/2}$, $x=N_0\pi kDt_m$, and $\alpha=N_0\pi kD/A$. Based on the agreement between the initial parts of experimental curves and those predicted theoretically using the two equations, the value for dimensionless parameter α was determined, and then the numerical values of constants D, N_0, A, and $J_0=AN_0$ were obtained. The related results are shown in Table 4 and Fig. 9. As is seen, the thiourea affects the nucleation rate constant, A, though blocks some of the active sites for nucleation. As a whole, the addition of thiourea leads to an increase in the stationary nucleation rate J_0, especially at lower potential.

Table 5 Vertical growth rate constants at various potentials and various thiourea concentrations, estimated at the steady-state current parts of current transients

Thiourea concentration (g L^{-1})	E (V)	I_{ss} (A cm^{-2})	K' (mol cm^{-2} s^{-1})
0	−0.95	0.043232	2.24×10^{-7}
	−1.00	0.090207	4.67×10^{-7}
0.02	−0.95	0.047357	2.45×10^{-7}
	−1.00	0.093949	4.87×10^{-7}
0.04	−0.95	0.053025	2.74×10^{-7}
	−1.00	0.095541	4.95×10^{-7}

The contribution to nucleus growth in the direction perpendicular to the substrate was also defined in a quantitative way. The transient current I_{ss} at steady-state conditions was used to evaluated the vertical growth rate constant K' ($I_{ss}=zFK'$), and the corresponding results are presented in Table 5 and Fig. 10. It is noted that the vertical growth rate of nucleus is also increased by the addition of thiourea.

Conclusion

Sulfur-bearing nickel was prepared by direct electrodeposition in an ammoniacal Ni(II) electrolyte containing thiourea. Static polarization behavior of the as-prepared sulfur-bearing nickels shows a high anodic dissolving activity in Watt bath. The surface microstructure of sulfur-bearing nickel strongly depends on the concentration of thiourea in electrolyte, and the increased thiourea concentration leads to finer grains. The as-prepared sulfur-bearing nickel has a face-centered cubic structure and (111) preferred orientation. The orientation distribution is strengthened, and more random

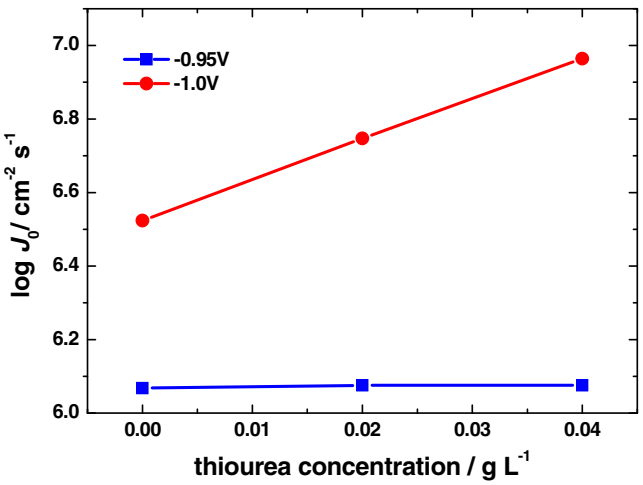

Fig. 9 Plots of log J_0 versus thiourea concentration at different applied potentials

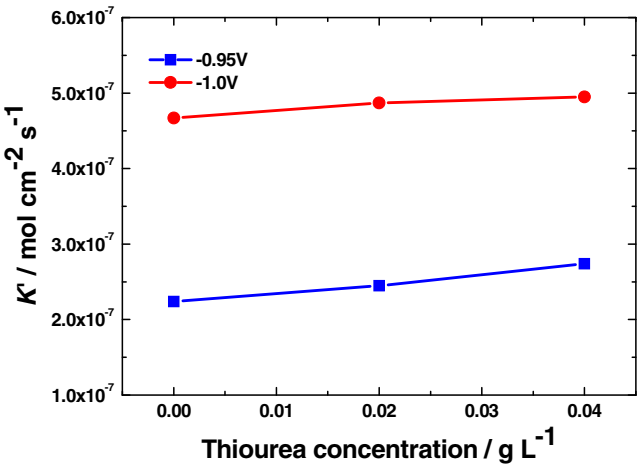

Fig. 10 Plots of K' versus thiourea concentration at different applied potentials

crystallographic texture is formed by the thiourea, which is beneficial to the anodic dissolution. Analysis of the initial parts of the transients allows the obtaining of the values of nucleation parameters, such as the nucleation rate constant, the number of active nucleation sites, and the stationary nucleation rate. Both the nucleation rate and the vertical growth rate are increased by the addition of thiourea.

Acknowledgments The authors would like to thank the Natural Science Foundation of China for financially supporting this research under contract no. 50040005.

References

1. Bear IJ, Flann RC, Mcdonald KJ, Rogers LJ, Woods R (1992) J Appl Electrochem 22:8–15
2. He HW, Liu HJ, Liu F, Zhou KC (2006) Surf Coat Technol 201:958–964
3. Gonzalez ER, Avaca LA, Tremiliosi-Filho G, Machado SAS, Ferreira M (1994) Int J Hydrogen Energy 19:17–21
4. Hine F, Yasuda M, Wang F, Yamakawa K (1971) Electrochim Acta 16:1519–1531
5. Paseka I (1993) Electrochim Acta 38:2449–2454
6. Sabela R, Paseka I (1990) J Appl Electrochem 20:500–505
7. Våland T, Burchardt T, Grøntoft T (2002) Int J Hydrogen Energy 27:39–44
8. Park KH, Mohapatra D, Reddy BR, Nam CW (2007) Hydrometallurgy 86:164–171
9. Bhuntumkomol K, Han KN, Lawson F (1982) Hydrometallurgy 8:147–160
10. Zheng GQ, Zheng LF, Cao HZ, Gao ZF, Ni SY, Zhang JY (2003) Trans Nonferrous Met Soc China 13:217–220
11. Danaee I, Shoghi F, Dehghani Mobarake M, Kameli M (2010) J Solid State Electrochem 14:57–62
12. Tsakova V (2008) J Solid State Electrochem 12:1421–1434
13. De Henau K, Huygens I, Strubbe K (2010) J Solid State Electrochem 14:83–91
14. Yang ZN, Zhang Z, Zhang JQ (2006) Surf Coat Technol 200:4810–4815
15. Hasse U, Fletcher S, Scholz F (2006) J Solid State Electrochem 10:833–840
16. Milchev A, Heerman L (2003) Electrochim Acta 48:2903–2913
17. Heerman L, Tarallo A (1999) J Electroanal Chem 470:70–76
18. Sluyters-Rehbach M, Wijenberg JHOJ, Bosco E, Sluyters JH (1987) J Electroanal Chem 23:1–20
19. Argañaraz MBQ, Vázquez CI, Lacconi GI (2010) J Electroanal Chem 639:95–101
20. Zheng GU, Cao HZ, Zheng LF (2007) J Appl Electrochem 37:799–803
21. Fletcher S, Gates D, Halliday CS, Lwin T, Nelson G, Westcott M (1983) J Electroanal Chem 159:267
22. Baskaran I, Sankara Narayanan TSN, Stephen A (2006) Mater Chem Phys 99:117–126
23. Bard AJ, Faulkner LR (2001) Electrochemical methods: fundamentals and applications. Wiley, New York
24. Scharifker BR, Hills GJ (1983) Electrochim Acta 28:879–889
25. Scharifker BR, Mostany J (1984) J Electroanal Chem 177:13–23